ACS Photonics

Article

Cite This: ACS Photonics 2019, 6, 395−402

pubs.acs.org/journal/apchd5

Optimal Nanoparticle Forces, Torques, and Illumination Fields

Yuxiang Liu,[†] Lingling Fan,[†,§] Yoonkyung E. Lee,[‡] Nicholas X. Fang,[‡] Steven G. Johnson,[¶,∥] and Owen D. Miller*[,†]

[†]Department of Applied Physics and Energy Sciences Institute, Yale University, New Haven, Connecticut 06511, United States
[§]School of Physics and National Laboratory of Solid State Microstructures, Nanjing University, Nanjing 210093, China
[‡]Department of Mechanical Engineering, Massachusetts Institute of Technology, Cambridge, Massachusetts 02139, United States
[¶]Department of Physics, Massachusetts Institute of Technology, Cambridge, Massachusetts 02139, United States
[∥]Department of Mathematics, Massachusetts Institute of Technology, Cambridge, Massachusetts 02139, United States

Supporting Information

ABSTRACT: A universal property of resonant subwavelength scatterers is that their optical cross-sections are proportional to a square wavelength, λ^2, regardless of whether they are plasmonic nanoparticles, two-level quantum systems, or RF antennas. The maximum cross-section is an intrinsic property of the *incident field*: plane waves, with infinite power, can be decomposed into multipolar orders with finite powers proportional to λ^2. In this article, we identify λ^2/c and λ^3/c as analogous force and torque constants, derived within a more general quadratic scattering-channel framework for upper bounds to optical force and torque for any illumination field. This framework also solves the reverse problem: computing globally optimal "holographic" incident beams, for a fixed collection of scatterers. We analyze structures and incident fields that approach the bounds, which for wavelength-scale bodies show a rich interplay between scattering channels, and we show that spherically symmetric structures are forbidden from reaching the plane-wave force/torque bounds. This framework should enable optimal mechanical control of nanoparticles with light.

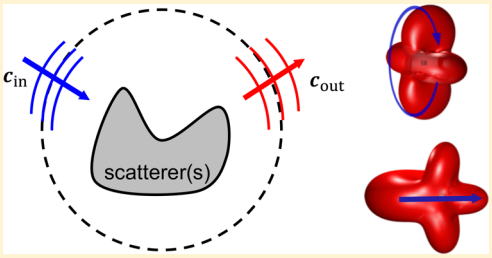

KEYWORDS: *optomechanics, optical force, optical torque, illumination fields, fundamental limits*

Optically induced forces and torques offer precise mechanical control of nanoparticles,[1−5] yet a basic understanding of what is possible has been limited by the inherent complexity in the optical response of a nanoparticle of any size, shape, and material. Here we show that a general scattering-channel decomposition embeds optical-response functions into matrix quadratic forms that, in tandem with a convex passivity constraint, readily yield *analytical* upper bounds for scatterers under arbitrary illumination. For plane waves, the force and torque bounds are proportional to λ^2/c and λ^3/c, respectively (for wavelength λ and speed of light c), for scatterers of any size, analogous to the well-known $\sim\lambda^2$ cross-section of a small scatterer.[6−11] Spheres, cylinders, and helices can approach the various bounds, which often require a complex interplay between scattering channels. With modern progress in spatial light modulators[12−14] and other beam-shaping techniques,[15−17] the "reverse" problem of shaping the incident field for a fixed geometry is increasingly important. Our quadratic-form framework naturally yields *globally* optimal illumination fields as extremal eigenvectors of Hermitian matrices. For a generic scattering problem, we show that optimized incident fields can achieve sizable enhancements (20−40×) to optically induced force and torque, offering orders-of-magnitude enhancements over conventional beams.

Mechanical forces induced by light are the foundation for optical trapping and manipulation, versatile tools with applications ranging from laser cooling[18] and nanoparticle guidance[5,19−25] to biomolecular sensing.[26−28] In the limit of dipolar response, analytical expressions for force and torque are known, as are associated concepts such as "gradient" forces[29−31] and optical "chirality".[32−34] At wavelength size scales and larger, the only structures for which analytical bounds or semianalytical response expressions are known are ray-optical[32,35] or spherical.[36] For nonspherical scatterers, optical forces and torques generally require simulation of Maxwell's equations,[37−41] providing numerical results but little insight. This contrasts strongly with the more detailed knowledge of *power* flow in such systems, ranging from bounds[6,7,10,11,42−44] to sum rules[45−47] to spherical-particle design criteria.[48] The disparity between the broad understanding of power flow versus the relative paucity for momentum flow may reflect the complexity of the Maxwell stress tensor relative to the Poynting vector. But as we show below, for passive systems in which energy is not supplied to the polarization currents, the requirement that outgoing power is less than incoming power is a convex constraint dictating what is possible for power, momentum, and other quantities of interest.

Received: September 7, 2018
Published: December 21, 2018

DOI: 10.1021/acsphotonics.8b01263
ACS Photonics 2019, 6, 395−402

"Holographic" optical force and torque generation[49−53] faces similar challenges. Whereas analytical bounds can be derived for the concentration of light for power transfer,[54] especially for dipolar objects,[55,56] finding optimal illumination fields for force/torque typically requires iterative computational optimization schemes[49,57,58] which may not converge to a global optimum. Recent work has identified the potential of quadratic forms for phase optimization,[58] "absorption"-like energy-exchange quantities,[59] or "optical eigenmodes";[60] the framework here shows generally how quadratic frameworks enable global optimization for any power quantity.

Reference 59 recently developed a framework that complements the one we use below. The authors identify conservation laws for "transfer" quantities, such as absorbed power, force, and torque, and derive upper bounds for such transfer rates. The bounds they derive for a given object are quite different from the analytical bounds that we derive for arbitrary scatterers: their bounds require the full scattering matrix of an object (as no other constraints are considered), whereas we use passivity as a constraint and derive bounds without knowledge of the scattering matrix, requiring only the number of incoming channels for which there is nontrivial coupling. The illumination bounds of ref 59 are closer to the bounds we derive for optimal illumination, with the key difference that our bounds apply generally to scattering quantities (scattered/extinguished power, linear momentum, angular momentum, etc.) that may not be "transfer" properties but that are necessarily quadratic forms.

SCATTERING-CHANNEL FRAMEWORK

The scattering properties of a body are uniquely determined by the incoming and outgoing fields on any bounding surface.[61] We represent all electromagnetic fields in six-dimensional tensors,

$$\psi = \begin{pmatrix} \mathbf{E} \\ \mathbf{H} \end{pmatrix} \tag{1}$$

For a fixed frequency ω (time-dependence $e^{-i\omega t}$), the "scattering channels" are basis sets on or outside a bounding surface of all scatterers in a given problem; equivalently, they are the "ports" commonly used in temporal coupled-mode theory.[62,63] We assume that the surface encloses all scatterers (such that all channels are propagating or far-field in nature), that the background is lossless, so that each channel carries fixed and position-independent energy and momenta, and that a finite set of channels describe the scattering process with arbitrarily high accuracy. We start by considering a basis of N "incoming" channels, represented by basis states φ_{1-} through φ_{N-} in a tensor $\mathbb{V}_-$:

$$\mathbb{V}_- = (\varphi_{1-}(x)\ \varphi_{2-}(x) \ldots \varphi_{N-}(x)) \tag{2}$$

Any complete set of incident channels may be used (plane waves, vector spherical waves, etc.). For the analytical force/torque bounds we will derive, the incident field will be fixed for a given problem, whereas for the illumination-field bounds, it will comprise the degrees of freedom to be optimized, in which case it is always possible to constrain the illumination to a subset of solid angles, as may be experimentally advantageous. From here, we will show how to construct sets of power-orthogonal incoming and outgoing states and that for any energy/momentum quantity there is a certain orthogonality between incoming and outgoing states that simplifies the ultimate quadratic forms.

The power flowing *into* a surface S with outward normal $\hat{\mathbf{n}}$ is given by

$$-\frac{1}{2}\mathrm{Re}\int_S \mathbf{E}\times\mathbf{H}^*\cdot\hat{\mathbf{n}} = -\frac{1}{4}\int_S \psi^\dagger \underbrace{\begin{pmatrix} & -\hat{\mathbf{n}}\times \\ \hat{\mathbf{n}}\times & \end{pmatrix}}_{\Theta}\psi \tag{3}$$

where Θ is a real-symmetric matrix (cross products change sign under interchange of their arguments, so $(\hat{\mathbf{n}}\times)^T = -\hat{\mathbf{n}}\times$ and vice versa). For the incoming-wave basis $\mathbb{V}_-$, with linearly independent but not necessarily orthonormal states, the power of an incoming field ψ_{in} in this basis, $\psi_{\mathrm{in}} = \mathbb{V}_-\mathbf{c}_{\mathrm{in}}$, is

$$\mathbf{c}_{\mathrm{in}}\left[\int_S \mathbb{V}_-^\dagger\left(-\frac{1}{4}\Theta\right)\mathbb{V}_-\right]\mathbf{c}_{\mathrm{in}} \tag{4}$$

Now we use the physical knowledge that $\mathbb{V}_-$ comprises only *incoming* states (with nonzero power) to assert that $-\Theta/4$ is *positive-definite* over all states of interest. Since $-\Theta/4$ is definite, it can be used to define a modified inner product, and then one can use, for example, the Gram−Schmidt process to orthonormalize our $\mathbb{V}_-$ basis in this quadratic form,[64] giving

$$\int_S \mathbb{V}_-^\dagger\left(-\frac{1}{4}\Theta\right)\mathbb{V}_- = \mathcal{I} \tag{5}$$

where $\mathcal{I}$ is the identity tensor. (Note that if the ambient medium is periodic, the surface S needs to be replaced by a volume that is one unit cell thick.[65] The Bloch waves in a periodic medium will not be linearly independent over a single cross-section.)

For power-orthogonal outgoing channels, we *time-reverse* the incoming channels. The outgoing channels, denoted $\mathbb{V}_+$, are then given by

$$\mathbb{V}_+ = \underbrace{\begin{pmatrix} \mathcal{I} & \\ & -\mathcal{I} \end{pmatrix}}_{\mathcal{P}}\mathbb{V}_-^* \tag{6}$$

where the parity matrix $\mathcal{P}$ accounts for the different time-reversal properties of electric ($\mathbf{E}\to\mathbf{E}^*$) and magnetic ($\mathbf{H}\to-\mathbf{H}^*$) fields. These states have the opposite normalization, because the power is flowing in the opposite direction:

$$\begin{aligned}\int_S \mathbb{V}_+^\dagger\left(-\frac{1}{4}\Theta\right)\mathbb{V}_+ &= \int_S \mathbb{V}_-^T\mathcal{P}\left(-\frac{1}{4}\Theta\right)\mathcal{P}\mathbb{V}_-^* \\ &= -\int_S \mathbb{V}_-^T\left(-\frac{1}{4}\Theta\right)\mathbb{V}_-^* \\ &= -\int_S \mathbb{V}_-^\dagger\left(-\frac{1}{4}\Theta\right)\mathbb{V}_-^* \\ &= -\mathcal{I}\end{aligned}$$

where we used the fact that $\mathcal{P}\Theta\mathcal{P} = -\Theta$, as can be verified by direct substitution. Thus, we have constructed power-orthonormal sets of incoming and outgoing states.

Any nontrivial field solution of a scattering solution will comprise both incoming and outgoing waves, and thus computing power, force, torque, or another quadratic form will include "overlap" terms between the incoming states of $\mathbb{V}_-$ and the outgoing states of $\mathbb{V}_+$. We can show generally that such terms will always cancel. Consider an energy/momentum-flux quantity that is a quadratic form of the fields flowing through a surface S:

DOI: 10.1021/acsphotonics.8b01263
ACS Photonics 2019, 6, 395−402

$$Q = \int_S \psi^\dagger Q \psi \tag{7}$$

where Q is a Hermitian operator determined by, for example, the Poyting vector or the electromagnetic stress tensor. In the SI, we use the time-reversal pairing of the input/output states to prove that Q must satisfy the time-reversal expression

$$Q = -\mathcal{P}Q^T\mathcal{P} \tag{8}$$

To show orthogonality between the incoming and outgoing waves, we now consider a scenario in which no absorption occurs, and all incoming power/momentum is converted into outgoing power/momentum. The total fields are given by the incoming and outgoing fields

$$\psi = \psi_{in} + \psi_{out} = \mathbb{V}_- \mathbf{c}_{in} + \mathbb{V}_+ \mathbf{c}_{out} \tag{9}$$

Evaluating the power/momentum quantity on the surface S, we find

$$\begin{aligned} Q &= \int_S [\psi_{in}^\dagger Q \psi_{in} + \psi_{out}^\dagger Q \psi_{out} + 2\mathrm{Re}\psi_{in}^\dagger Q \psi_{out}] \\ &= \mathbf{c}_{in}^\dagger \left(\int_S \mathbb{V}_-^+ Q \mathbb{V}_- \right) \mathbf{c}_{in} + \mathbf{c}_{out}^\dagger \left(\int_S \mathbb{V}_+^\dagger Q \mathbb{V}_+ \right) \mathbf{c}_{out} \\ &\quad + 2\mathrm{Re}\left[\mathbf{c}_{in}^\dagger \left(\int_S \mathbb{V}_-^\dagger Q \mathbb{V}_- \right) \mathbf{c}_{out} \right] \end{aligned} \tag{10}$$

From eq 8, it is straightforward to show that incoming/outgoing channels carry equal and opposite energy/momentum: $\int_S \mathbb{V}_+^\dagger Q \mathbb{V}_+ = -\int_S \mathbb{V}_-^\dagger Q \mathbb{V}_-$. Thus, the first two terms in eq 10 add to zero, and we are left only with the third term. The total sum Q has to equal zero, leaving

$$\mathrm{Re} \int_S \mathbb{V}_-^\dagger Q \mathbb{V}_+ = 0 \tag{11}$$

Thus, the time-reversed, propagating basis states exhibit orthogonality between incoming and outgoing waves, for any flux quantity represented by a quadratic form.

■ ANALYTICAL BOUNDS

By virtue of linearity, any quantity describing energy or momentum flow of a field ψ through a surface S can be described by eq 7, as a quadratic form.[41,66] We can decompose the incoming- and outgoing-wave components of ψ into basis-coefficient vectors $\mathbf{c}_{in}$ and $\mathbf{c}_{out}$:

$$\psi_{in}(x) = \mathbb{V}_-(x)\mathbf{c}_{in} \tag{12a}$$

$$\psi_{out}(x) = \mathbb{V}_+(x)\mathbf{c}_{out} \tag{12b}$$

For linear materials (considered hereafter), the basis coefficients $\mathbf{c}_{in}$ and $\mathbf{c}_{out}$ are related by $\mathbf{c}_{out} = \mathbb{S}\mathbf{c}_{in}$, where $\mathbb{S}$ is the scattering matrix. By the power-orthonormalization condition for $\mathbb{V}_-$, eq 5, and its negative for $\mathbb{V}_+$, absorption is simply

$$P_{abs} = \mathbf{c}_{in}^\dagger \mathbf{c}_{in} - \mathbf{c}_{out}^\dagger \mathbf{c}_{out} \tag{13}$$

i.e., incoming minus outgoing power. Similarly, the force or torque on any scatterer, in some direction i, is the difference in momentum flux of the incoming and outgoing waves, given by

$$F_i = \frac{1}{c}[\mathbf{c}_{in}^\dagger \mathbb{P}_i \mathbf{c}_{in} - \mathbf{c}_{out}^\dagger \mathbb{P}_i \mathbf{c}_{out}] \tag{14}$$

$$\tau_i = \frac{1}{\omega}[\mathbf{c}_{in}^\dagger \mathbb{J}_i \mathbf{c}_{in} - \mathbf{c}_{out}^\dagger \mathbb{J}_i \mathbf{c}_{out}] \tag{15}$$

where c is the speed of light and $\mathbb{P}_{ii}$ and $\mathbb{J}_i$ are dimensionless matrix measures of linear and angular momentum, given by overlap integrals (described above) involving the stress tensor (SI). There are no cross terms, as proven by eq 11. Equations 13−15 compactly represent enegy/momentum flow in an intuitive basis. We can derive general bounds by adding a single constraint: passivity.

Passivity requires that induced currents do no work;[67] as a consequence, absorption and scattered power are nonnegative. In a recent series of papers,[42−44,68−70] we have identified passivity-based quadratic constraints to the currents induced within a medium and applied them to find material-dictated bounds to a variety of optical-response functions. Here, we apply such constraints to the scattering channels themselves. Nonnegative absorption, i.e., $P_{abs} > 0$, translates eq 13 to a quadratic photon-conservation constraint on $\mathbf{c}_{out}$:

$$\mathbf{c}_{out}^\dagger \mathbf{c}_{out} \le \mathbf{c}_{in}^\dagger \mathbf{c}_{in} \tag{16}$$

The largest force or torque that can be exerted on a nanoparticle can thus be formulated as the maximum of eqs 14 and 15 subject to passivity, i.e., eq 16. Equations 14−16 represent a particularly straightforward quadratic optimization with quadratic constraints. Of the two terms each in eqs 14 and 15, the first are fixed by the incident field, while the second are the variable ones to be bounded. For simplicity, we assume the standard case in which channels have equal positive- and negative-momentum eigenstates, such that the eigenvalues come in positive/negative pairs and $\max[\mathbf{c}_{out}^\dagger(-\mathbb{Q})\mathbf{c}_{out}] = \max[\mathbf{c}_{out}^\dagger \mathbb{Q} \mathbf{c}_{out}]$ (it is straightforward to generalize the results for alternative bases). Then the Rayleigh quotient[64] in tandem with the passivity constraint, eq 16, bounds the second terms of eqs 14 and 15 by $\mathbf{c}_{out}^\dagger \mathbb{Q} \mathbf{c}_{out} \le (\mathbf{c}_{out}^\dagger \mathbf{c}_{out}) \lambda_{max}(\mathbb{Q}) \le (\mathbf{c}_{in}^\dagger \mathbf{c}_{in}) \lambda_{max}(\mathbb{Q})$, for $\mathbb{Q} = \mathbb{P}_i, \mathbb{J}_i$, where $\lambda_{max}(\mathbb{Q})$ is the largest eigenvalue of $\mathbb{Q}$. Denoting the incoming power, momentum flow, and angular momentum flow by $\mathcal{W}_{in} = \mathbf{c}_{in}^\dagger \mathbf{c}_{in}$, $\mathcal{P}_{in,i} = \mathbf{c}_{in}^\dagger \mathbb{P}_i \mathbf{c}_{in}/c$, and $\mathcal{J}_{in,i} = \mathbf{c}_{in}^\dagger \mathbb{J}_i \mathbf{c}_{in}/\omega$, respectively, the maximum force and torque are given by

$$F_i \le \mathcal{P}_{in,i} + \frac{\mathcal{W}_{in}}{c} \lambda_{max}(\mathbb{P}_i) \tag{17}$$

$$\tau_i \le \mathcal{J}_{in,i} + \frac{\mathcal{W}_{in}}{\omega} \lambda_{max}(\mathbb{J}_i) \tag{18}$$

Equations 17 and 18 are general bounds to the force or torque that can be exerted on any scatterer, given only the incident-field properties and the power and momentum properties of the relevant scattering channels. Intuitively, eq 17 predicts an optimal force for nanoparticles that absorb all of the momentum along direction i of the coupled incoming channels and generate outgoing waves in those channels of equal power and large, negative momentum. The eigenvalue encodes the relative difficulty in any set of scattering channels of generating such momentum transfer. The analogous interpretation applies to eq 18 in terms of angular momentum.

Natural scattering channels for wavelength-scale nanoparticles are the vector spherical waves (VSWs), $\mathbf{M}_{l,m}^{\pm}$ (TE) and $\mathbf{N}_{l,m}^{\pm}$ (TM), where l and m are the angular and projected quantum numbers, respectively. A scatterer of finite size will have nontrivial coupling to only a finite number of channels

DOI: 10.1021/acsphotonics.8b01263
ACS Photonics 2019, 6, 395−402

parametrized by l_{max}, a maximum angular quantum number. Farsund and Felderhof[71] have derived analytical expressions for the integrals defining the matrices $\mathbb{P}_i$ and $\mathbb{J}_i$ (see SI). As shown in Figure 1, $\mathbb{J}_z$ is diagonal, since the VSWs are pure angular

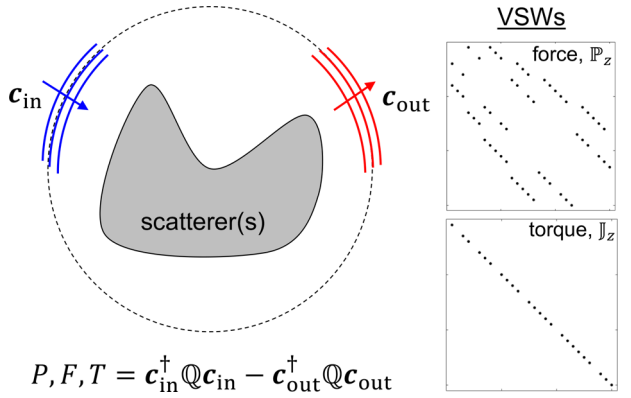

Figure 1. Power, force, or torque imparted to any structure (or collection thereof) can be encoded in matrix quadratic forms $\mathbb{Q}$ that are amenable to analytical bounds and quadratic optimization. In a vector-spherical-wave (VSW) basis, the force ($\mathbb{Q} \to \mathbb{P}_i$) and torque ($\mathbb{Q} \to \mathbb{J}_z$) matrices have nonzero values as shown on the right.

momentum states. Conversely, $\mathbb{P}_z$ has nonzero entries only off the diagonal. In the SI, we derive bounds on the largest eigenvalues of $\mathbb{P}_i$ and $\mathbb{J}_i$: $\lambda_{max}(\mathbb{P}_i) \le 1$ and $\lambda_{max}(\mathbb{J}_i) = l_{max}$. The physical origin of these bounds can be understood as follows: for any linear combination of VSWs comprising a single photon, they will demonstrate less directionality (and hence smaller linear momentum) than the corresponding plane-wave photon with momentum $\hbar\mathbf{k}$; by contrast, the angular momentum of a VSW can be as large as l_{max} times $\hbar|\mathbf{k}|$ per photon. We can simplify eqs 17 and 18 for prototypical plane-wave incident fields. Within channels up to l_{max}, a plane wave with amplitude $\mathbf{E}_0$ and wavevector $\mathbf{k}$ carries power $\mathbf{c}_{in}^\dagger \mathbf{c}_{in} = \pi(l_{max}^2 + 2l_{max})\frac{|\mathbf{E}_0|^2}{2Z_0|\mathbf{k}|^2}$ (SI). Its linear momentum flux per time is $\mathcal{P}_{in,i} = \mathbf{c}_{in}^\dagger \mathbb{P}_i \mathbf{c}_{in}/c = \frac{\beta_i}{c}\frac{l_{max}}{l_{max}+1}\mathbf{c}_{in}^\dagger \mathbf{c}_{in}$, where $\beta_i = \hat{\mathbf{k}}\cdot\hat{\mathbf{i}}$ is the fraction of the incident wave's momentum in direction i. Its angular momentum per time is $\mathcal{J}_{in,i} = \mathbf{c}_{in}^\dagger \mathbb{J}_i \mathbf{c}_{in}/\omega = (\beta_i\gamma_i/\omega)\mathbf{c}_{in}^\dagger \mathbf{c}_{in}$, where γ_i is the degree of right circular polarization for the wave projected into direction i. Both β_i and γ_i have a range of $[-1, 1]$. Following this procedure and dividing out the plane-wave intensity, $I_{inc} = |\mathbf{E}_0|^2/2Z_0$, yields the bounds

$$\frac{F_i}{I_{inc}} \le \frac{\lambda^2}{4\pi c}(l_{max}^2 + 2l_{max})\left(1 + \beta_i \frac{l_{max}}{l_{max}+1}\right) \quad (19)$$

$$\frac{\tau_i}{I_{inc}} \le \frac{\lambda^3}{8\pi^2 c}(l_{max}^2 + 2l_{max})(l_{max} + \beta_i\gamma_i) \quad (20)$$

Equations 19 and 20 bound the largest forces/torques that can be generated from incident plane waves. (Equations 17 and 18 provide bounds for more general incident waves.) The quantities λ^2/c and λ^3/c naturally emerge as force/torque analogs of the λ^2 scattering cross-sections. Such proportionalities emerge physically by dimensional analysis, while the quadratic framework leading to eqs 19 and 20 provides exact, quantitative upper bounds.

Within eqs 19 and 20 is a second interesting result: spherically symmetric scatterers *cannot* reach the plane-wave incident-field bounds, except in the trivial case $l_{max} = 1$. Reaching these bounds requires outgoing waves to be proportional to the maximal eigenvectors of the $\mathbb{P}_i$ and $\mathbb{J}_i$ matrices, which do not coincide with the incoming-wave coefficients of a plane wave. (By modifying the incident field to match the VSW coefficients over the full 4π angular range, one can engineer a scenario in which spherically symmetric objects are optimal.) This is in contrast to scattered-power optimization, where it is known that spherically symmetric scatterers can be globally optimal[72] for *any* incident field, and it arises because the additional requirements of directionality/polarization for linear/angular momentum require specific combinations of VSW channels for maximum effect.

Figures 2 and 3 show examples of designed nanoparticles that can approach the plane-wave bounds. For Figure 2, the inner

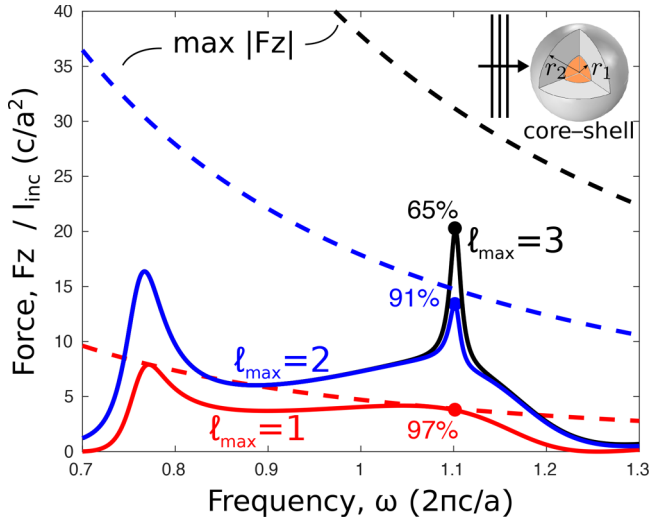

Figure 2. Force bounds of eqs 17 and 19 require strong and highly directional scattering. Core–shell structures with aligned resonances show strong scattering and imperfect but good directionality. Optimized Si–SiO_2 structures ($r_1 = 0.1a$, $r_2 = 0.9a$) experience a force approaching the $l_{max} = 3$ bounds, with negligible scattering in higher channels.

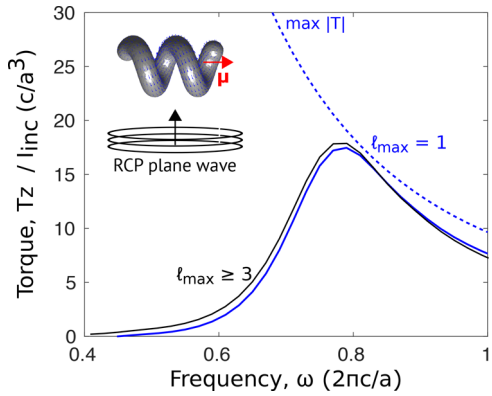

Figure 3. To achieve the torque bounds of eqs 18 and 20, a scatterer must generate the largest possible Δm between incoming/outgoing waves. A helix interacting with a circularly polarized wave impinging normal to its rotation axis exhibits a magnetic dipole moment μ that generates counter-rotating outgoing waves, to create a torque (solid lines) that nearly achieves the $l_{max} = 1$ bound (dotted lines).

DOI: 10.1021/acsphotonics.8b01263
ACS Photonics 2019, 6, 395–402

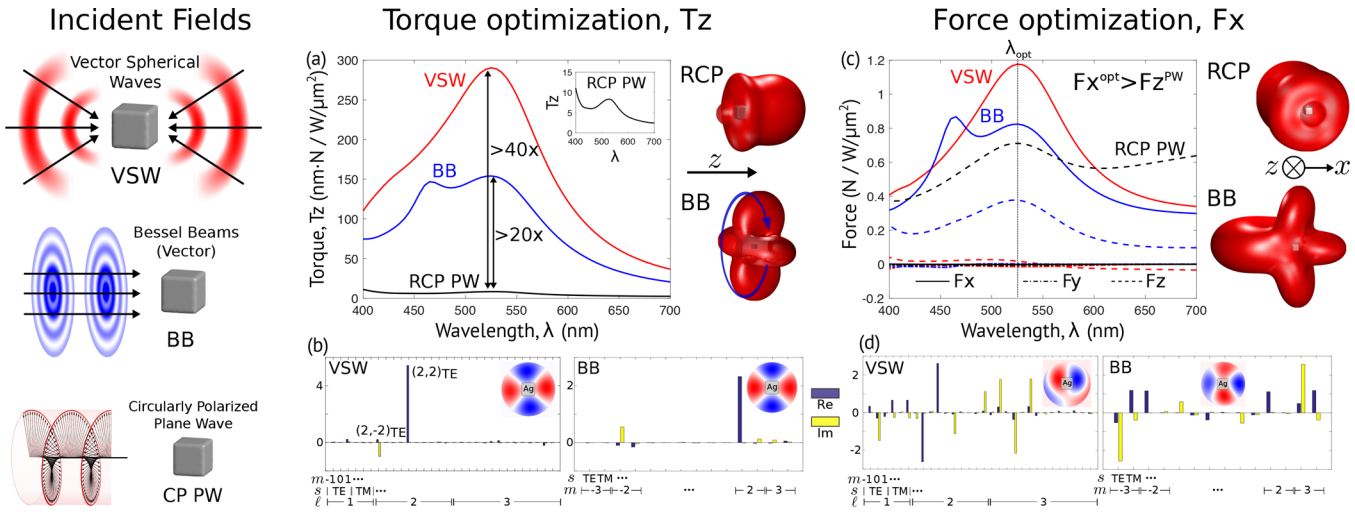

Figure 4. Global optimization of an illumination field can be achieved in a single eigenvector computation per eq 23. Here we optimize force and torque on a silver cube (200 nm edge length) for illumination fields decomposed into VSW and Bessel-beam (BB) bases, with circularly polarized plane waves (CP PWs) as a standard for comparison (left). (a) Despite the seemingly large torque generated on resonance ($\lambda = 525$ nm) by a RCP PW (black line and inset), optimal VSW and BB incident fields offer >40× and >20× improvements, respectively, for a fixed field intensity. The scattered fields (right) for the optimal BB show an outgoing radiation pattern carrying angular momentum, primarily in the $l = 2$, $m = \pm 2$ channels. (c) Plane waves generate no *in-plane* forces (F_x, F_y) on such a cube. VSW and BB incident fields optimized for maximum $|F_x|$ generate in-plane forces larger than the F_z of a plane wave. The scattered fields (right) for the optimal BB show the highly asymmetric radiation pattern. (b, d) Optimized VSW and BB field coefficients, alongside field patterns in the plane of the cube (insets).

radii of core−shell Si−SiO_2 structures were optimized (over a length scale a) to exhibit aligned resonances ("superscattering"[7]). Even though spheres cannot exactly reach the bounds, as proven above, such resonances can effectively scatter light in the backward direction, enhancing a large force in the forward direction that achieves a substantial fraction of the bound. For the three channels primarily excited, nearly 65% of the total bound can be achieved, while nearly saturating the force due to the $l = 1, 2$ channels. By contrast, spheres cannot generate substantial torque, which requires coupling positive- and negative-angular-momentum channels. Helices are excellent nanoswimmers,[73] and we find that illuminating a helix (refractive index 3.5, structural details in SI) *normal* to its rotation axis generates counter-rotating outgoing waves and a large net torque perpendicular to its rotation axis. Figure 3 shows that an optimized helix can closely approach the $l_{max} = 1$ bound.

OPTIMAL ILLUMINATION FIELDS

The quadratic framework lends itself readily to the reverse problem: given a fixed scatterer, what incident field generates maximal force/torque? More generally, what incident field maximizes general power/momentum quadratic forms? Significant interest in this problem has led to a variety of iterative optimization methods, which often converge to suboptimal local extrema.[57] Yet starting from the Poynting-vector/stress-tensor quadratic form, described by eq 7, one can write any figure of merit in the form

$$Q = \begin{pmatrix} \mathbf{c}_{in} \\ \mathbf{c}_{out} \end{pmatrix}^{\dagger} \begin{pmatrix} \mathbb{Q}_{11} & \mathbb{Q}_{12} \\ \mathbb{Q}_{12}^{\dagger} & \mathbb{Q}_{22} \end{pmatrix} \begin{pmatrix} \mathbf{c}_{in} \\ \mathbf{c}_{out} \end{pmatrix} \tag{21}$$

where $\mathbb{Q}_{11}$ and $\mathbb{Q}_{22}$ (and hence the whole $\mathbb{Q}$ matrix) are Hermitian. Per eqs 13−15, for absorbed power, net force, and net torque, the off-diagonal terms are zero, while $\mathbb{Q}_{11} = -\mathbb{Q}_{22} = \mathbb{I}, \mathbb{P}_i$, and $\mathbb{J}_i$, respectively (where $\mathbb{I}$ is the identity matrix). For the power or momentum flux in the scattered field, the precise definitions of $\mathbb{Q}_{ii}$ depend on the decomposition of the incident field into incoming versus outgoing waves; in the VSW basis, one can show (cf. SI) that $\mathbb{Q}_{12} = -\mathbb{Q}_{11} = -\mathbb{Q}_{22} = \mathbb{I}, \mathbb{P}_i$, or $\mathbb{J}_i$, respectively. The outgoing-field coefficients are given by the product of the scattering matrix with the incoming-field coefficients, $\mathbb{S}\mathbf{c}_{in}$, such that one can rewrite eq 21 as a quadratic form of the incoming-field coefficients only:

$$Q = \mathbf{c}_{in}^{\dagger}[\mathbb{Q}_{11} + \mathbb{Q}_{12}\mathbb{S} + \mathbb{S}^{\dagger}\mathbb{Q}_{12}^{\dagger} + \mathbb{S}^{\dagger}\mathbb{Q}_{22}\mathbb{S}]\mathbf{c}_{in} \tag{22}$$

Constraining the total power contained in the incoming wave over some spatial region or set of channels imposes a constraint $\mathbf{c}_{in}^{\dagger}\mathbb{A}\mathbf{c}_{in} \leq 1$ for a Hermitian positive-definite matrix $\mathbb{A}$ (e.g., $\mathbb{A}$ is the identity matrix for a unity-average-power constraint in the scattering channels). The optimal coefficient vector $\mathbf{c}_{in}^{(opt)}$ that maximizes eq 22 subject to this constraint solves the generalized eigenproblem

$$[\mathbb{Q}_{11} + 2\mathrm{Re}(\mathbb{Q}_{12}\mathbb{S}) + \mathbb{S}^{\dagger}\mathbb{Q}_{22}\mathbb{S}]\mathbf{c}_{in}^{(opt)} = \lambda_{max}\mathbb{A}\mathbf{c}_{in}^{(opt)} \tag{23}$$

where λ_{max} is the largest eigenvalue. The extremal eigenfunction solving eq 23 is the globally optimal incident field. Intuitively, it is sensible that the scattering matrix $\mathbb{S}$ determines the optimal incident field, since $\mathbb{S}$ encodes the response for any incoming wave. A key feature of eq 23 is that for the wavelength-scale scatterers in many optical force experiments, only a small to moderate number of VSWs are typically excited. Hence $\mathbb{S}$ has relatively few degrees of freedom, enabling rapid computation of the optimal incident field.

Figure 4 demonstrates the capability for eq 23 to generate orders-of-magnitude increases in force/torque through wavefront shaping. We consider a 200 nm silver nanocube. The nanocube supports a strongly scattering quadrupole resonance at wavelength $\lambda = 525$ nm that already generates a significant force along the direction of an incoming plane wave. For a right circularly polarized (RCP) wave, absorption in the silver transfers the $m = 1$ angular momentum of the wave to the

DOI: 10.1021/acsphotonics.8b01263
ACS Photonics 2019, 6, 395−402

cube and generates a commensurate torque (a, inset). Yet through wavefront shaping, the torque can be dramatically enhanced, without increasing the intensity of the incident field. We consider two incident-field bases: VSWs, with quantum numbers l, m, and s (where s denotes polarization), and vector Bessel beams (BBs),[74] diffraction-free cylindrical beams with an angular order m and a polarization s. Note that Bessel beams are a subset of VSWs, so VSWs can exhibit superior performance, although BBs are more practical for experimental implementations.[31] One could similarly optimize plane waves coming from within a given solid angle. After solving for the scattering matrix with a free-software implementation[75] of the boundary element method,[76] solution of eq 23 yielded the optimal VSW and BB fields. As shown in Figure 4(a,b), isolation and optimization of the dominant scattering channels yields 20−40× increases in the torque. The field patterns (right) indicate the angular momentum carried away by the scattered fields. In contrast to the torque case, the nanocube already feels large forces in plane-wave interactions, as seen in Figure 4(c) (black dashed line), simply through the momentum carried in forward-scattered and backscattered waves (i.e., along z). However, the force in a lateral direction is necessarily zero by symmetry. With the same nanocube scattering matrix, we thus optimized eq 23 for the x-directed force [Figure 4(c)]. The optimal field coefficients, shown in Figure 4(d), generate lateral forces even larger than the normally directed force under plane-wave excitation. The field patterns (right, red) show the highly asymmetric scattering that is responsible for the large lateral force.

The quadratic-optimization approach developed here can be applied across the landscape of optical force and torque generation. The analytical bounds of eqs 17−20 predict optimal response for a fixed incident field, while the optimal-eigenvector approach of eq 23 determines optimal incident fields for a fixed structure. Looking forward, incorporation of temporal dynamics and associated effects (e.g., back-action[77]) may lead to robust and efficient methods for producing even larger effects, toward optimal dynamical control at the nanoscale.

■ ASSOCIATED CONTENT

Supporting Information

The Supporting Information is available free of charge on the ACS Publications website at DOI: 10.1021/acsphotonics.8b01263.

Details of the scattering-channel framework and resulting quadratic forms; vector-spherical-wave definitions, properties, and matrices; eigenvalue bounds; helix-structure details; cross-section bounds rederived (PDF)

■ AUTHOR INFORMATION

Corresponding Author

*E-mail: owen.miller@yale.edu.

ORCID

Owen D. Miller: 0000-0003-2745-2392

Notes

The authors declare no competing financial interest.

■ ACKNOWLEDGMENTS

The authors thank Chia-Wei Hsu and Ognjen Ilic for helpful discussions. Y.L. and O.D.M. were supported by the Air Force Office of Scientific Research under award number FA9550-17-1-0093. L.F. was supported by a Shanyuan Overseas scholarship from the Hong Kong Shanyuan Foundation at Nanjing University. S.G.J. was supported in part by the Army Research Office under contract number W911NF-13-D-0001. N.F. was supported by the Air Force Office of Scientific Research (AFOSR) Multidisciplinary Research Program of the University Research Initiative (MURI) and from KAUST-MIT agreement #2950.

■ REFERENCES

(1) Grier, D. G. A revolution in optical manipulation. *Nature* **2003**, *424*, 810−816.

(2) Neuman, K. C.; Block, S. M. Optical trapping. *Rev. Sci. Instrum.* **2004**, *75*, 2787−2809.

(3) Hänggi, P.; Marchesoni, F. Artificial Brownian motors: Controlling transport on the nanoscale. *Rev. Mod. Phys.* **2009**, *81*, 387−442.

(4) Juan, M. L.; Righini, M.; Quidant, R. Plasmon nano-optical tweezers. *Nat. Photonics* **2011**, *5*, 349−356.

(5) Ilic, O.; Kaminer, I.; Lahini, Y.; Buljan, H.; Soljačić, M. Exploiting Optical Asymmetry for Controlled Guiding of Particles with Light. *ACS Photonics* **2016**, *3*, 197−202.

(6) Hamam, R. E.; Karalis, A.; Joannopoulos, J. D.; Soljačić, M. Coupled-mode theory for general free-space resonant scattering of waves. *Phys. Rev. A: At., Mol., Opt. Phys.* **2007**, *75*, 053801.

(7) Ruan, Z.; Fan, S. Design of subwavelength superscattering nanospheres. *Appl. Phys. Lett.* **2011**, *98*, No. 043101.

(8) Loudon, R. *The Quantum Theory of Light*, 3rd ed.; Oxford University Press: New York, 2000.

(9) Stutzman, W. L.; Thiele, G. A. *Antenna Theory and Design*, 3rd ed.; John Wiley & Sons, 2012.

(10) Kwon, D.-H.; Pozar, D. M. Optimal Characteristics of an Arbitrary Receive Antenna. *IEEE Trans. Antennas Propag.* **2009**, *57*, 3720−3727.

(11) Liberal, I.; Ra'di, Y.; Gonzalo, R.; Ederra, I.; Tretyakov, S. A.; Ziolkowski, R. W. Least Upper Bounds of the Powers Extracted and Scattered by Bi-anisotropic Particles. *IEEE Trans. Antennas Propag.* **2014**, *62*, 4726−4735.

(12) Arrizón, V.; Ruiz, U.; Carrada, R.; González, L. A. Pixelated phase computer holograms for the accurate encoding of scalar complex fields. *J. Opt. Soc. Am. A* **2007**, *24*, 3500.

(13) Herández-Herández, R. J.; Terborg, R. A.; Ricardez-Vargas, I.; Volke-Sepúlveda, K. Experimental generation of Mathieu-Gauss beams with a phase-only spatial light mod- ulator. *Appl. Opt.* **2010**, *49*, 6903.

(14) Clark, T. W.; Offer, R. F.; Franke-Arnold, S.; Arnold, A. S.; Radwell, N. Comparison of beam generation techniques using a phase only spatial light modulator. *Opt. Express* **2016**, *24*, 6249.

(15) Karimi, E.; Piccirillo, B.; Nagali, E.; Marrucci, L.; Santamato, E. Efficient generation and sorting of orbital angular momentum eigenmodes of light by thermally tuned q- plates. *Appl. Phys. Lett.* **2009**, *94*, 231124.

(16) Schulz, S. A.; Machula, T.; Karimi, E.; Boyd, R. W. Integrated multi vector vortex beam generator. *Opt. Express* **2013**, *21*, 16130−141.

(17) Chen, C. F.; Ku, C. T.; Tai, Y. H.; Wei, P. K.; Lin, H. N.; Huang, C. B. Creating Optical Near-Field Orbital Angular Momentum in a Gold Metasurface. *Nano Lett.* **2015**, *15*, 2746−2750.

(18) Metcalf, H. J.; van der Straten, P. *Laser Cooling and Trapping*; Springer: New York, NY, 1999.

(19) Ashkin, A. Acceleration and Trapping of Particles by Radiation Pressure. *Phys. Rev. Lett.* **1970**, *24*, 156−159.

(20) Allen, L.; Barnett, S. M.; Padgett, M. J. *Optical Angular Momentum*; CRC Press, 2003.

(21) Bonin, K.; Kourmanov, B.; Walker, T. Light torque nanocontrol, nanomotors and nanorockers. *Opt. Express* **2002**, *10*, 984−989.

(22) Pelton, M.; Liu, M.; Kim, H. Y.; Smith, G.; Guyot-Sionnest, P.; Scherer, N. F. Optical trapping and alignment of single gold nanorods by using plasmon resonances. *Opt. Lett.* **2006**, *31*, 2075−2077.

DOI: 10.1021/acsphotonics.8b01263
ACS Photonics 2019, 6, 395−402

(23) Tong, L.; Miljković, V. D.; Käll, M. Alignment, rotation, and spinning of single plas- monic nanoparticles and nanowires using polarization dependent optical forces. *Nano Lett.* **2010**, *10*, 268−273.
(24) Dholakia, K.; Čižmár, T. Shaping the future of manipulation. *Nat. Photonics* **2011**, *5*, 335−342.
(25) Wang, K.; Schonbrun, E.; Steinvurzel, P.; Crozier, K. B. Trapping and rotating nanoparticles using a plasmonic nano-tweezer with an integrated heat sink. *Nat. Commun.* **2011**, *2*, 466−469.
(26) Eriksson, E.; Scrimgeour, J.; Granéli, A.; Ramser, K.; Wellander, R.; Enger, J.; Hanstorp, D.; Goksör, M. Optical manipulation and microfluidics for studies of single cell dynamics. *J. Opt. A: Pure Appl. Opt.* **2007**, *9*, S113−S121.
(27) Jonáš, A.; Zemánek, P. Light at work: The use of optical forces for particle manipulation, sorting, and analysis. *Electrophoresis* **2008**, *29*, 4813−4851.
(28) Wang, X.; Chen, S.; Kong, M.; Wang, Z.; Costa, K. D.; Li, R. A.; Sun, D. Enhanced cell sorting and manipulation with combined optical tweezer and microfluidic chip tech- nologies. *Lab Chip* **2011**, *11*, 3656.
(29) Ashkin, A.; Dziedzic, J. M.; Bjorkholm, J. E.; Chu, S. Observation of a single-beam gradient force optical trap for dielectric particles. *Opt. Lett.* **1986**, *11*, 288.
(30) Nieto-Vesperinas, M.; Sáenz, J. J.; Gómez-Medina, R.; Chantada, L. Optical forces on small magnetodielectric particles. *Opt. Express* **2010**, *18*, 11428−11443.
(31) Jones, P. H.; Maragò, O. M.; Volpe, G. *Optical Tweezers: Principles and Applications*; Cambridge University Press, 2015.
(32) Barron, L. D. *Molecular Light Scattering and Optical Activity*; Cambridge University Press, 2004.
(33) Tang, Y.; Cohen, A. E. Optical chirality and its interaction with matter. *Phys. Rev. Lett.* **2010**, *104*, 163901.
(34) Bliokh, K. Y.; Nori, F. Characterizing optical chirality. *Phys. Rev. A: At., Mol., Opt. Phys.* **2011**, *83*, No. 021803R.
(35) Ashkin, A. Forces of a single-beam gradient laser trap on a dielectric sphere in the ray optics regime. *Biophys. J.* **1992**, *61*, 569−582.
(36) Rahimzadegan, A.; Alaee, R.; Fernandez-Corbaton, I.; Rockstuhl, C. Fundamental lim- its of optical force and torque. *Phys. Rev. B: Condens. Matter Mater. Phys.* **2017**, *95*, No. 035106.
(37) Waterman, P. C. Symmetry, unitarity, and geometry in electromagnetic scattering. *Phys. Rev. D: Part. Fields* **1971**, *3*, 825−839.
(38) Mishchenko, M. I.; Travis, L. D.; Mackowski, D. W. T-matrix computations of light scattering by nonspherical particles: A review. *J. Quant. Spectrosc. Radiat. Transfer* **1996**, *55*, 535−575.
(39) Doicu, A.; Wriedt, T.; Eremin, Y. A. *Light Scattering by Systems of Particles: Null-Field Method with Discrete Sources: Theory and Programs*; Springer, 2006; Vol. *124*.
(40) Nieminen, T. A.; Loke, V. L. Y.; Stilgoe, A. B.; Knöner, G.; Brańczyk, A. M.; Heckenberg, N. R.; Rubinsztein-Dunlop, H. Optical tweezers computational toolbox. *J. Opt. A: Pure Appl. Opt.* **2007**, *9*, S196−S203.
(41) Reid, M. T. H.; Johnson, S. G. Efficient Computation of Power, Force, and Torque in BEM Scattering Calculations. *IEEE Trans. Antennas Propag.* **2015**, *63*, 3588−3598.
(42) Miller, O. D.; Polimeridis, A. G.; Homer Reid, M. T.; Hsu, C. W.; DeLacy, B. G.; Joannopoulos, J. D.; Soljačić, M.; Johnson, S. G. Fundamental limits to optical response in absorptive systems. *Opt. Express* **2016**, *24*, 3329−3364.
(43) Yang, Y.; Miller, O. D.; Christensen, T.; Joannopoulos, J. D.; Soljačić, M. Low-loss Plasmonic Dielectric Nanoresonators. *Nano Lett.* **2017**, *17*, 3238−3245.
(44) Miller, O. D.; Ilic, O.; Christensen, T.; Reid, M. T. H.; Atwater, H. A.; Joannopoulos, J. D.; Soljačić, M.; Johnson, S. G. Limits to the Optical Response of Graphene and Two-Dimensional Materials. *Nano Lett.* **2017**, *17*, 5408−5415.
(45) Gordon, R. G. Three Sum Rules for Total Optical Absorption Cross Sections. *J. Chem. Phys.* **1963**, *38*, 1724.
(46) Purcell, E. M. On the Absorption and Emission of Light by Interstellar Grains. *Astrophys. J.* **1969**, *158*, 433−440.
(47) Sohl, C.; Gustafsson, M.; Kristensson, G. Physical limitations on broadband scattering by heterogeneous obstacles. *J. Phys. A: Math. Theor.* **2007**, *40*, 11165−11182.
(48) Grigoriev, V.; Bonod, N.; Wenger, J.; Stout, B. Optimizing nanoparticle designs for ideal absorption of light. *ACS Photonics* **2015**, *2*, 263−270.
(49) Polin, M.; Ladavac, K.; Lee, S.-H.; Roichman, Y.; Grier, D. G. Optimized holographic optical traps. *Opt. Express* **2005**, *13*, 5831−45.
(50) Grier, D. G.; Roichman, Y. Holographic optical trapping. *Appl. Opt.* **2006**, *45*, 880−887.
(51) Martín-Badosa, E.; Montes-Usategui, M.; Carnicer, A.; Andilla, J.; Pleguezuelos, E.; Juvells, I. Design strategies for optimizing holographic optical tweezers set-ups. *J. Opt. A: Pure Appl. Opt.* **2007**, *9*, S267−S277.
(52) Bianchi, S.; Di Leonardo, R. Real-time optical micro-manipulation using optimized holograms generated on the GPU. *Comput. Phys. Commun.* **2010**, *181*, 1444−1448.
(53) Taylor, M. A.; Waleed, M.; Stilgoe, A. B.; Rubinsztein-Dunlop, H.; Bowen, W. P. Enhanced optical trapping via structured scattering. *Nat. Photonics* **2015**, *9*, 669−673.
(54) Sheppard, C. J. R.; Larkin, K. G. Optimal concentration of electromagnetic radiation. *J. Mod. Opt.* **1994**, *41*, 1495−1505.
(55) Gerhardt, I.; Wrigge, G.; Bushev, P.; Zumofen, G.; Pfab, R.; Sandoghdar, V. Strong extinction of a laser beam by a single molecule. *Phys. Rev. Lett.* **2007**, *98*, No. 033601.
(56) Zumofen, G.; Mojarad, N. M.; Sandoghdar, V.; Agio, M. Perfect Reflection of Light by an Oscillating Dipole. *Phys. Rev. Lett.* **2008**, *101*, 180404.
(57) Lee, Y. E.; Miller, O. D.; Reid, M. T. H.; Johnson, S. G.; Fang, N. X. Computational inverse design of non-intuitive illumination patterns to maximize optical force or torque. *Opt. Express* **2017**, *25*, 6757−6766.
(58) Taylor, M. A. Optimizing phase to enhance optical trap stiffness. *Sci. Rep.* **2017**, *7*, 555.
(59) Fernandez-Corbaton, I.; Rockstuhl, C. Unified theory to describe and engineer conser- vation laws in light-matter interactions. *Phys. Rev. A* **2018**, *95*, 1−13.
(60) Mazilu, M.; Baumgartl, J.; Kosmeier, S.; Dholakia, K. Optical Eigenmodes; exploiting the quadratic nature of the light-matter interaction. *Opt. Express* **2011**, *19*, 933.
(61) Jin, J.-M. *Theory and Computation of Electromagnetic Fields*; John Wiley & Sons, 2011.
(62) Newton, R. G. *Scattering Theory of Waves and Particles*; Springer Science & Business Media, 2013.
(63) Suh, W.; Wang, Z.; Fan, S. Temporal coupled-mode theory and the presence of non- orthogonal modes in lossless multimode cavities. *IEEE J. Quantum Electron.* **2004**, *40*, 1511−1518.
(64) Horn, R. A.; Johnson, C. R. *Matrix Analysis*, 2nd ed.; Cambridge University Press: New York, NY, 2013.
(65) Johnson, S. G.; Bienstman, P.; Skorobogatiy, M. A.; Ibanescu, M.; Lidorikis, E.; Joannopoulos, J. D. Adiabatic theorem and continuous coupled-mode theory for efficient taper transitions in photonic crystals. *Phys. Rev. E: Stat. Phys., Plasmas, Fluids, Relat. Interdiscip. Top.* **2002**, *66*, 66608.
(66) Jackson, J. D. *Classical Electrodynamics*, 3rd ed.; John Wiley & Sons, 1999.
(67) Welters, A.; Avniel, Y.; Johnson, S. G. Speed-of-light limitations in passive linear media. *Phys. Rev. A: At., Mol., Opt. Phys.* **2014**, *90*, No. 023847.
(68) Miller, O. D.; Johnson, S. G.; Rodriguez, A. W. Shape-Independent Limits to Near-Field Radiative Heat Transfer. *Phys. Rev. Lett.* **2015**, *115*, 204302.
(69) Yang, Y.; Massuda, A.; Roques-Carmes, C.; Kooi, S. E.; Christensen, T.; Johnson, S. G.; Joannopoulos, J. D.; Miller, O. D.; Kaminer, I.; Soljačić, M. Maximal spontaneous photon emission and energy loss from free electrons. *Nat. Phys.* **2018**, *14*, 894−899.
(70) Shim, H.; Fan, L.; Johnson, S. G.; Miller, O. D. Fundamental limits to near-field optical response, over any bandwidth. *arXiv:1805.02140*, 2018.

DOI: 10.1021/acsphotonics.8b01263
ACS Photonics 2019, 6, 395−402

(71) Farsund, Ø.; Felderhof, B. U. Force, torque, and absorbed energy for a body of arbitrary shape and constitution in an electromagnetic radiation field. *Phys. A* **1996**, *227*, 108−130.
(72) Miroshnichenko, A. E.; Tribelsky, M. I. Ultimate Absorption in Light Scattering by a Finite Obstacle. *Phys. Rev. Lett.* **2018**, *120*, No. 033902.
(73) Walker, D.; Kübler, M.; Morozov, K. I.; Fischer, P.; Leshansky, A. M. Optimal Length of Low Reynolds Number Nanopropellers. *Nano Lett.* **2015**, *15*, 4412−4416.
(74) Novitsky, A. V.; Novitsky, D. V. Negative propagation of vector Bessel beams. *J. Opt. Soc. Am. A* **2007**, *24*, 2844.
(75) Reid, M. T. H. scuff-EM: Free, open-source boundary-element software. http://homerreid.com/scuff-EM.
(76) Harrington, R. F. *Field Computation by Moment Methods*; IEEE Press: Piscataway, NJ, 1993.
(77) Juan, M. L.; Gordon, R.; Pang, Y.; Eftekhari, F.; Quidant, R. Self-induced back-action optical trapping of dielectric nanoparticles. *Nat. Phys.* **2009**, *5*, 915−919.

DOI: 10.1021/acsphotonics.8b01263
ACS Photonics 2019, 6, 395−402